ACS BIO & MED CHEM Au
AN OPEN ACCESS JOURNAL OF THE AMERICAN CHEMICAL SOCIETY

pubs.acs.org/biomedchemau

Article

Cell-Penetrating D-Peptides Retain Antisense Morpholino Oligomer Delivery Activity

Carly K. Schissel, Charlotte E. Farquhar, Annika B. Malmberg, Andrei Loas, and Bradley L. Pentelute*

Cite This: *ACS Bio Med Chem Au* 2022, 2, 150−160

Read Online

ACCESS | Metrics & More | Article Recommendations | Supporting Information

ABSTRACT: Cell-penetrating peptides (CPPs) can cross the cell membrane to enter the cytosol and deliver otherwise nonpenetrant macromolecules such as proteins and oligonucleotides. For example, recent clinical trials have shown that a CPP attached to phosphorodiamidate morpholino oligomers (PMOs) resulted in higher muscle concentration, increased exon skipping, and dystrophin production relative to another study of the PMO alone in patients of Duchenne muscular dystrophy. Therefore, effective design and the study of CPPs could help enhance therapies for difficult-to-treat diseases. So far, the study of CPPs for PMO delivery has been restricted to predominantly canonical L-peptides. We hypothesized that mirror-image D-peptides could have similar PMO delivery activity as well as enhanced proteolytic stability, facilitating their characterization and quantification from biological milieu. We found that several enantiomeric peptide sequences could deliver a PMO−biotin cargo with similar activities while remaining stable against serum proteolysis. The biotin label allowed for affinity capture of fully intact PMO−peptide conjugates from whole-cell and cytosolic lysates. By profiling a mixture of these constructs in cells, we determined their relative intracellular concentrations. When combined with PMO activity, these concentrations provide a new metric for delivery efficiency, which may be useful for determining which peptide sequence to pursue in further preclinical studies.

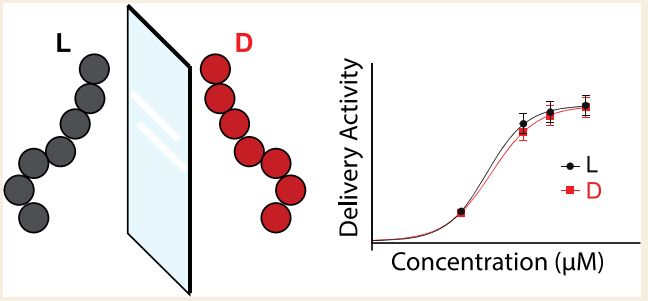

KEYWORDS: *cell-penetrating peptides, mirror-image peptides, PMO, oligonucleotides, delivery*

INTRODUCTION

Cell-penetrating peptides (CPPs) can help treat disease by enhancing the delivery of cell-impermeable cargo. CPPs are a class of peptides that are capable of directly entering the cell cytosol.[1−3] These sequences can deliver covalently bound cargo, offering therapeutic potential to macromolecules otherwise restricted to extracellular targets. Although CPPs have been widely studied since their discovery, the field lacks a robust methodology to quantify cell entry and penetration efficacy. This dearth of knowledge is due to the complicated mechanisms of CPP cell entry and the many variables that affect CPP efficacy in any given assay—such as peptide concentration, cell type, temperature, treatment time, and cargo.[4] For example, for the well-studied CPP penetratin (RQIKIWFQNRRMKWKK), the reported ratio between intracellular and extracellular concentration ranges from 0.6:1.0 to 95.0:1.0.[5,6] In addition, it is challenging to determine subcellular localization once a peptide is internalized, despite advances in fluorescence, immunoblot, and mass spectrometry detection.[7] The choice of CPP−cargo adds an additional confounding factor, as studies in our laboratory have demonstrated that the cell-penetrating ability of more than 10 common CPPs differs when bound to a cyanine dye versus a macromolecular drug, with no discernable trend.[8] Therefore, the effective development of CPPs requires a new methodology for understanding CPP cell entry and subcellular localization that can be carried out on the CPP−cargo conjugate.

A therapeutic macromolecule that would benefit from enhanced delivery is phosphorodiamidate morpholino oligomer (PMO), which has recently reached the market as an antisense "exon skipping" therapy for Duchenne muscular dystrophy (DMD). One of the drugs, eteplirsen, is a 10 kDa synthetic antisense oligomer that must reach the nucleus and bind pre-mRNA for its therapeutic effect. However, studies have shown that two-thirds of eteplirsen is cleared renally within 24 h of administration.[9,10] Several CPPs have been shown to increase PMO uptake, and recent clinical trial results have shown that once monthly dosing of SRP-5051 resulted in higher muscle concentration, increased exon skipping, and dystrophin production at 12 weeks as compared to once

Received: November 1, 2021
Revised: December 14, 2021
Accepted: December 15, 2021
Published: February 16, 2022

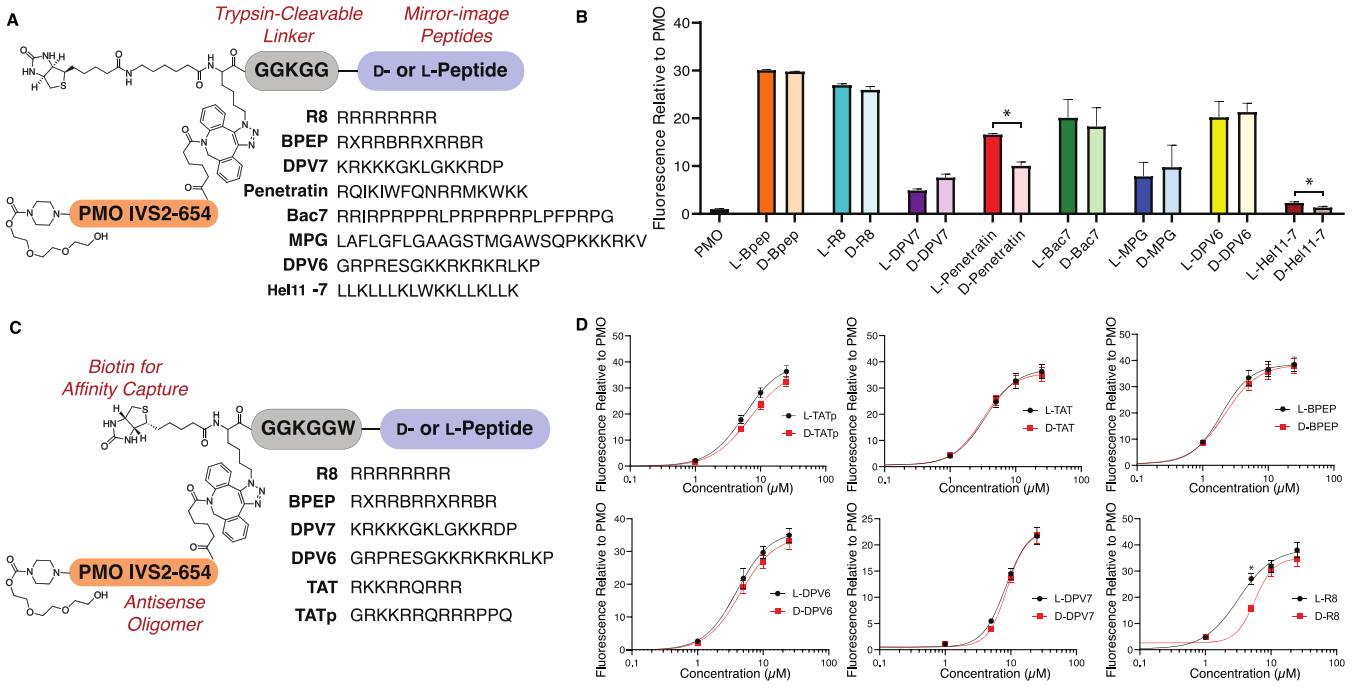

Figure 1. Mirror-image cell-penetrating peptides have a similar PMO delivery activity as their native counterparts. (A) Construction of the first-generation conjugates studied, including the eight studied CPP sequences. Macromolecular cargo PMO IVS2-654 is attached to the N-terminus of the peptides, along with a biotin handle for subsequent affinity capture. A trypsin-cleavable linker connects the cargo to the peptides, and a 6-aminohexanoic acid moiety is between the biotin and the peptide. (B) Activity data from the EGFP 654 assay conducted with D- and L-form of the first-generation sequences at 5 μM. (C) Construction of the second-generation conjugates used in subsequent experiments. The aminohexanoic acid linker was removed and each peptide contains a single tryptophan residue for quantitation by UV−vis. (B) Dose−response curves of D- and L-form of several sequences at varying concentrations. No membrane toxicity was observed after analyzing the supernatant of these experiments (SI). Bars and points represent mean ± SD; $N = 3$ distinct samples from a representative biological replicate. Replicate experiments showed similar results and are shown in the SI. Statistical significance between the D- and L-sample at each concentration was determined using a two-tailed unpaired t-test and indicated by $^*p < 0.01$, with blank indicating not statistically significant.

weekly dosing of eteplirsen after 24 weeks in a different study.[11] Although a wide variety of CPPs have been tested for PMO delivery, they have been limited to the native L-form and studied predominantly with an activity-based assay, forgoing quantitative information on the amount of material inside the cell.[12]

Because PMO is proteolytically stable and invisible to the immune system,[10] attachment to an L-peptide may disrupt the desirable characteristics of PMO; however, conjugates using mirror-image peptides may retain these characteristics.[13−15] D-Peptides have been explored as CPPs and have been found to display at times greater activities to their L-counterparts, despite suggested chiral binding interactions between CPPs and the cell membrane.[16,17] A study on TAT endosomalytic peptide analogues found that the full D-form decreased uptake but enhanced endosomal escape and proteolytic stability compared to the native form.[15,18] Another study reported that a cyclic D-peptide, when coadministered with insulin, enhanced its oral bioavailability and therapeutic effect in the gut.[19] Some reports are contentious as to whether mutations to D-amino acids are detrimental to CPP activity, and certainly CPPs that depend on a chiral interaction or highly ordered structure to enter the membrane would lose efficacy from D-amino acid substitutions.[20,21] Previous studies have suggested that efficient CPPs for PMO delivery lack secondary structure and can enter the cell through clathrin-mediated endocytosis.[22,23] While it has been found that PMO-D-CPPs have enhanced proteolytic stability over their L-counterparts,[24] their PMO delivery activity has not been investigated. In addition to their underexplored potential, we are interested in studying D-CPPs as potential therapeutic carrier moieties because their fully noncanonical sequence is resistant to proteolysis and may go unrecognized by the host immune system.[15,20] Despite this potential, mirror-image peptides have not yet been fully explored for the delivery of PMO.

The proteolytic stability of mirror-image peptides would simplify their characterization after uptake into cells, providing orthogonal information to activity-based assays. Currently, the main method used to characterize PMO−CPP internalization is an in vitro assay in which successful delivery of the active oligomer to the nucleus results in green fluorescence.[25] While this is an excellent assay to measure PMO−CPP activity, this assay does not give information on the quantity of material inside the cell. Especially for conjugates with a known endocytic mechanism, understanding endosomal escape is crucial. High concentrations of peptides trapped in the endosome would not be apparent by the activity assay alone, but this loss of active peptide could be of great therapeutic detriment.[26] Therefore, an additional assay that reveals relative quantities of material in different parts of the cell would provide a valuable metric of CPP delivery, in parallel with our current activity assay. This could be achieved by extracting the cytosolic fraction of treated cells using a mild detergent, such as digitonin, and comparison to the whole-cell fraction.[27] Comparing activity and relative quantity would be a valuable metric for efficiency, where a high-efficiency peptide is one with a high ratio of antisense activity to internal concentration.

https://doi.org/10.1021/acsbiomedchemau.1c00053
ACS Bio Med Chem Au 2022, 2, 150−160

Existing methods to quantify uptake into cells include fluorescence, immunoblot, and mass spectrometry, but it is still challenging to distinguish between endosomal and cytosolic localization. Several assays can differentiate between endosomal and cytosolic localization using indirect quantification via a readout generated by a delivered cargo, including the chloroalkane penetration assay (CAPA),[28] GFP complementation assays,[29] and more recently the NanoClick[30] assay and SLEEQ[31] assay. Direct quantification of the cytosolic concentration of a fluorescently labeled protein construct is possible using fluorescence correlation spectroscopy.[32]

Mass spectrometry is a direct quantification tool that would give information about the concentration of peptides recovered from biological mixtures with limited labeling required. Past studies have illustrated how matrix-assisted laser desorption ionization time-of-flight (MALDI-TOF) mass spectrometry is a practical tool for the absolute and relative quantification of peptides and proteins. For example, using an internal standard of a similar molecular weight is sufficient for the generation of a calibration curve.[33] Quantitation of total uptake of L-CPPs was achieved using heavy-atom-labeled internal standards.[34,35] While this assay provided information regarding whole-cell uptake of CPPs and CPP−peptide conjugates, it is limited by the need for heavy-atom labeling and the rapid degradation of L-peptides.[36] A method for circumnavigating the need for spike-in of heavy-atom-labeled standards was developed for the relative quantification of phosphopeptides.[37] However, the proteolytic stability of D-peptides would facilitate their recovery and analysis as a mixture from inside cells and animals, allowing for the use of a new metric of antisense delivery efficiency.

Here, we report that compared to the native L-forms, the mirror-image forms of several sequences were equally able to deliver antisense molecules to the nucleus, but their increased proteolytic stability simplified mass spectrometry-based characterization following cytosolic delivery. Cytosolic delivery can be quantified based on the recovery of intact constructs from inside the cell. We profiled the uptake of biotinylated CPPs and PMO−CPPs to determine their relative concentrations in the whole cell and cytosol using careful extraction with digitonin and direct detection via MALDI-TOF. By comparing PMO delivery activity to relative internal concentration, we can derive a new metric for cargo delivery efficiency that may be useful for the future development of CPPs for PMO delivery.

RESULTS AND DISCUSSION

Mirror-Image Peptides Have the Same PMO Delivery Activity as Native Forms

We first established that several mirror-image peptides could deliver a model PMO molecule to the nucleus of cells with similar efficacy to their native L-forms. We selected commonly studied cationic peptides with precedented PMO delivery activity, but not known for their dependence on secondary structure or receptor interaction, and synthesized them in their L- and D-forms. The first iteration of these constructs contained a biotin linked through a 6-aminohexanoic acid residue and a trypsin-cleavable motif between the peptide and the cargo. The cargo portion contained an azide for conjugation to PMO and a biotin for use in affinity capture (Figure 1A). The second generation of these constructs did not include an aminohexanoic acid linker and did include a single tryptophan residue for quantitation by UV−vis (Figure 1C). The final constructs contained at least five cationic residues and included oligoarginine (R8, BPEP, Bac7, TAT, TATp) and amphipathic (Penetratin, Hel11-7, DPV6, DPV7, MPG) sequences.

In total, 14 PMO−peptide sequences were synthesized in their D- and L-forms and tested in an activity-based in vitro assay.[22,23] To synthesize constructs, L-peptides were synthesized via automated fast-flow peptide synthesis, and D-peptides were synthesized using semiautomated fast-flow peptide synthesis (SI). Azido-lysine and biotin moieties were added to the N-terminus of the peptides manually, and the peptides were simultaneously cleaved and deprotected before purification via RP-HPLC. PMO was modified with a dibenzocyclooctyne (DBCO) moiety and purified before attachment to azido-peptides via strain-promoted azide-alkyne cycloaddition in water. Purified constructs were then tested using an activity-based readout in which nuclear delivery results in fluorescence. Briefly, HeLa cells stably transfected with an EGFP gene interrupted by a mutated intron of β-globin (IVS2-654) produce a nonfluorescent EGFP protein. The successful delivery of PMO IVS2-654 to the nucleus results in corrective splicing and EGFP synthesis. The amount of PMO delivered to the nucleus is therefore correlated with EGFP fluorescence, quantified by flow cytometry. Activity is reported as mean fluorescence intensity (MFI) relative to PMO alone. This activity assay provides indirect information on how much active PMO is delivered to the nucleus.

Dose−response studies with sequences in the D- and L-form confirmed similar activities between mirror-image CPPs. From our initial proof-of-concept experiment, involving eight sequences in L- and D-form tested at a single concentration (5 μM), there was not a significant difference between the activities of mirror-image peptides with the exception of penetratin and Hel11-7 (Figure 1B, SI). PMO-D-penetratin and PMO-D/L-Hel11-7 demonstrated some toxicity and were discontinued from study (SI). The second-generation constructs (Figure 1C) were tested at varying concentrations in the EGFP 654 assay, and the results further suggested that mirror-image peptides shared nearly identical PMO delivery activities (Figure 1D, SI). Interestingly, while PMO-D-R8 showed similar activity to PMO-L-R8, it did not demonstrate the closeness of activity observed with the other sequences. The trend has been observed before, albeit without attached cargos, in that L-R8 entered cells more efficiently than D.[20] Though striking similarities were observed for the selected peptides, this similarity is certainly not expected for all CPPs and cargoes, including those that rely on the secondary structure or receptor-mediated uptake. Furthermore, the supernatant from these assays was tested for lactate dehydrogenase (LDH) release, indicative of membrane toxicity, and it was confirmed that constructs did not elicit membrane toxicity at the doses tested (SI). These activities correspond with how much PMO is delivered to the nucleus but do not provide information regarding the total amount of material inside the cell. The relative efficiency of a PMO−CPP could be characterized by comparing the activity to internal concentration, as discussed later (Figure 2).

Mirror-Image Peptides Are Proteolytically Stable

Our primary motivation for investigating mirror-image peptides for transporting PMO was that the D-form would be stable against proteolysis and thus would match this property of the PMO cargo. D-peptides are indeed stable

https://doi.org/10.1021/acsbiomedchemau.1c00053
ACS Bio Med Chem Au 2022, 2, 150−160

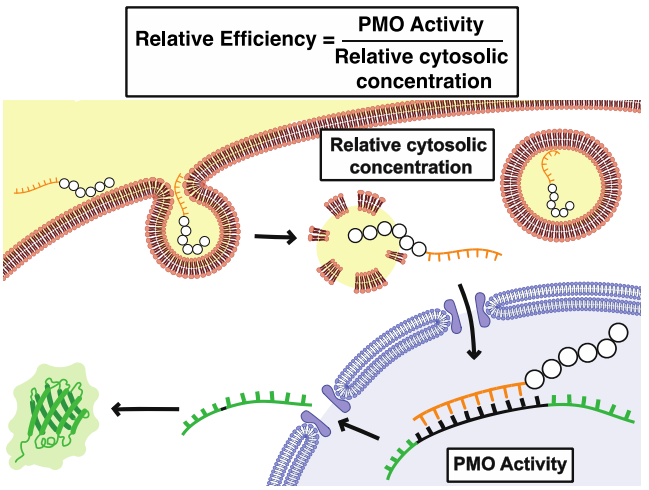

Figure 2. Schematic of how PMO−CPPs may enter the cell to perform exon-skipping activity. While activity assays give information of how much active PMO reached its target, a mass spectrometry-based assay may give information on the amount of PMO−CPP located in the cell and cytosol. Comparing these metrics provides a new estimate of CPP efficiency.

against degradation, as illustrated by a time-course study in which both forms of PMO−CPPs were incubated in 25% human serum. While the studied PMO-D-CPPs remained intact 24 h later, L-forms rapidly degraded into multiple fragments, leaving the parent construct as a minor product after only 1 h of incubation (Figure 3). The major degradation products correspond to loss of the C-terminal RRRPPQ and KKRRQRRRPPQ motifs of TATp (sequence: GGKGGWGRKKRRQRRRPPQ). Similar observations were noted for DPV6, DPV7, and BPEP (SI). This observation furthers the notion that L-peptides are not suitable for investigation using mass spectrometry after recovery from a biological setting. However, D-peptide conjugates can be recovered from a biological environment such as serum without suffering degradation, simplifying their characterization via mass spectrometry.

Mirror-Image PMO−Peptides Can Be Recovered from Inside Cells

The proteolytic stability of D-peptides simplifies the recovery of the mixtures of intact constructs after being internalized into cells. While MALDI-ToF has been used previously to analyze the quantity of L-peptides and protein−peptide conjugates recovered from inside cells, it has not yet been used to profile PMO-D-peptides or the mixtures of more than three conjugates at a time.[34,35] MALDI-ToF has also been used to quantify many different delivered cargos, rather than the CPP.[38−40] The use of D-peptides would facilitate the analysis of a mixture of conjugates because without degradation, only the parent peak would be observed. Moreover, this platform has not yet been used to study peptides recovered from subcellular fractions.

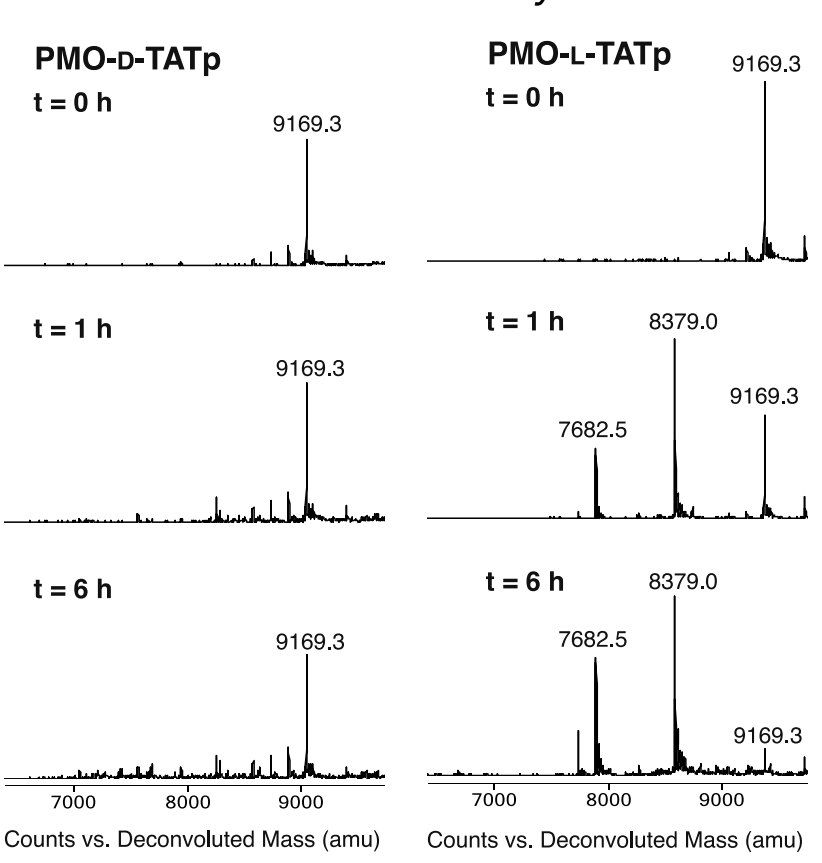

Figure 3. Mirror-image cell-penetrating peptides remain proteolytically stable. Mass spectra of PMO-D- and L-conjugates following incubation with 25% human serum. The L-variant is degraded within 1 h, while the D-variant is stable after 6 h. Spectra from other PMO−CPPs are shown in the Supporting Information.

https://doi.org/10.1021/acsbiomedchemau.1c00053
ACS Bio Med Chem Au 2022, 2, 150−160

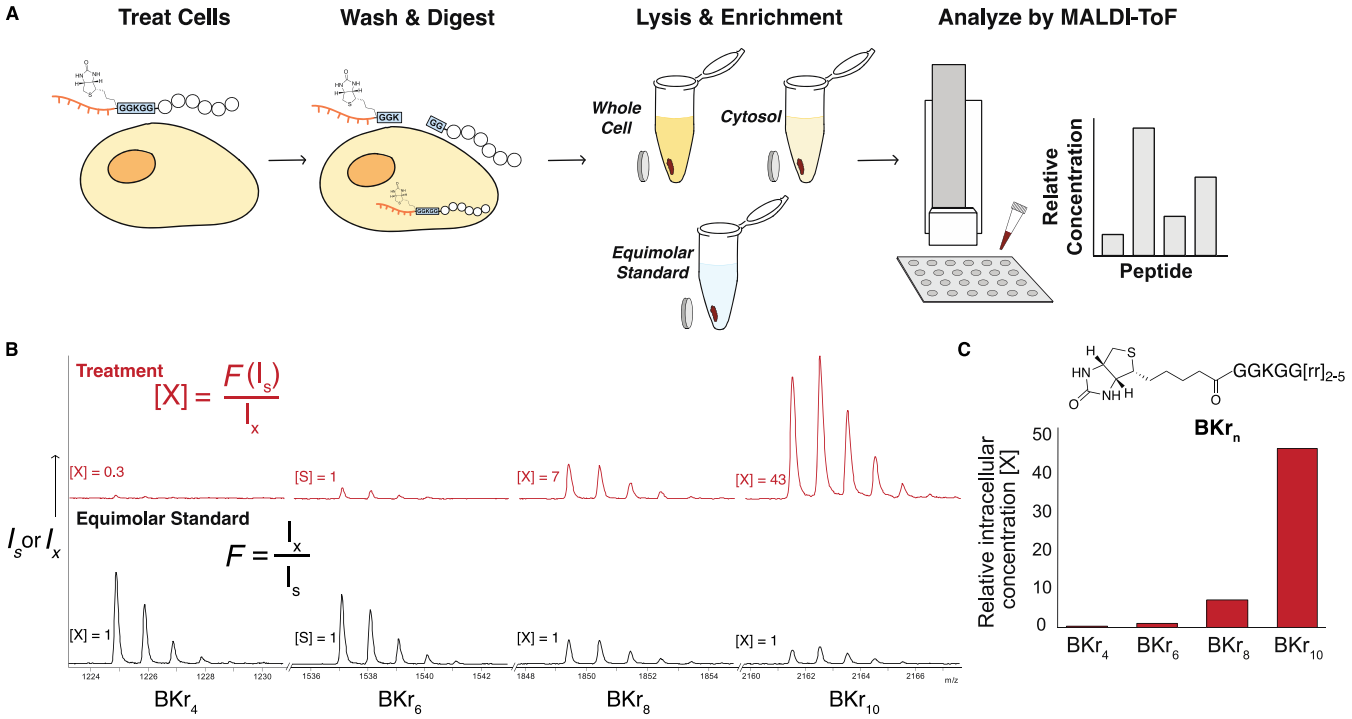

Figure 4. Uptake assay reveals relative concentrations of intact construct inside the cell. (A) Workflow of the uptake assay; cells are treated with PMO-D-CPPs, washed, and lysed to extract the whole-cell lysate or the cytosol. A trypsin-cleavable L-linker ensures extracellular constructs are not recovered. Constructs are immobilized on magnetic streptavidin beads, washed, and plated directly for MALDI analysis. Intensities of analytes compared to an equimolar standard provide relative concentrations. (B) MALDI-TOF mass spectra displaying ions of intact biotinylated D-polyarginine peptides, isolated after internalization into HeLa cells. Spectra show ions corresponding to intact conjugates in the equimolar spike-in (black) and the whole-cell lysate of cells treated with an equimolar mixture (red). (C) By comparing relative intensities in the equimolar standard, the response factor (F) was determined and used to calculate the fold change in concentration in the experimental samples, shown as a bar graph, normalized to BKr_4. Also shown is the equation used to determine the relative concentration: I (intensity), [X] (sample concentration), F (response factor), X (sample), and S (standard).

Through a series of experiments, we show that the mixtures of intact PMO-D-CPPs can be recovered from the cytosol of cells and analyzed by MALDI-ToF to estimate their relative abundances without the need for isotope labeling or standard curves (Figure 4A).

Our first step was to recapitulate a known empirical trend that more Arg residues lead to greater uptake. We began our assay with a simple model system of four polyarginine peptides with a trypsin-cleavable linker and a single biotin label. HeLa cells were incubated with biotin-K-D-Arg_4, D-Arg_6, D-Arg_8, and D-Arg_{10} for 1 h. The cells were then washed extensively with PBS and heparin and trypsinized to lift the cells as well as to cleave the L-linker on extracellular constructs, preventing their recovery. The treatment with heparin is known to release peptides bound to the membrane but that are not internalized,[20] although it is possible that membrane-bound peptides are recovered in the whole-cell lysate. Moreover, we confirmed that the GGKGG trypsin-cleavable linker cleaves fully within 5 min of trypsin treatment (SI). The whole-cell lysate was then prepared using RIPA buffer. Fully intact biotinylated peptides were captured with magnetic streptavidin Dynabeads, washed, and plated directly for MALDI analysis. Also plated were Dynabeads incubated in an equimolar mixture of the same constructs as determined by UV−vis (Figure 4B).

The relative concentration of peptides on beads can be estimated by determining the analyte's response factor (F) from the equimolar standard (Figure 4B). In the standard, each analyte's concentration is 1 mM, and each analyte's response factor (F) is determined by normalizing their intensities to an internal standard (S). Here, BKr_6 was selected as the arbitrary standard, where F = 1. The response factor of each analyte should remain consistent across samples that contain the same analytes[33,37] and was used to calculate the fold change in concentration in the experimental samples. The relative concentrations [X] of analytes, normalized to the "internal standard" BKr_6, are shown as a bar graph (Figure 4C). There is a clear increase in the concentration of constructs with more Arg residues, with BKr_{10} having 40-fold greater concentration than BKr_6. This trend of the greater number of Arg residues leading to greater uptake is already well documented in the literature.[41,42]

PMO-D-CPPs Can Be Extracted from Cytosol and Analyzed by MALDI-TOF

Next, we found that these PMO−CPP constructs likely enter via energy-dependent endocytosis. When evaluating CPP delivery efficiency, considering the mechanism of uptake and potential for endosomal entrapment is necessary. In contrast with CPPs alone that can enter via passive diffusion,[41,43] we hypothesized that the uptake mechanism of these constructs was likely endocytosis, considering the size of the PMO cargo as well as previous studies that we have conducted on similar conjugates.[22,23] Using a panel of chemical endocytosis inhibitors, we performed a pulse-chase EGFP 654 assay format in which cells were preincubated with inhibitors before treatment with the L- and D-form of PMO-DPV7 and PMO-Bac7 (SI). Analysis by flow cytometry revealed that

https://doi.org/10.1021/acsbiomedchemau.1c00053
ACS Bio Med Chem Au 2022, 2, 150−160

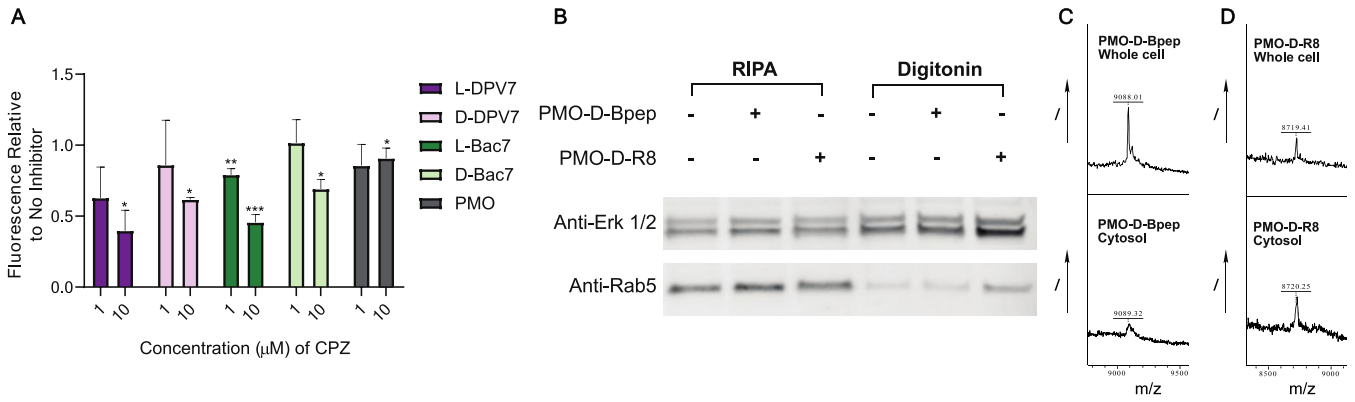

Figure 5. PMO-D-CPPs enter via endocytosis and can be detected in whole-cell and cytosolic lysates by MALDI-TOF. (A) PMO activities from an EGFP 654 assay in which cells are treated in a pulse-chase format with chemical endocytosis inhibitors followed by PMO conjugates at 5 μM. Chlorpromazine (CPZ) produces a dose-dependent inhibition of PMO activity. Bars represent group mean ± SD, $N = 3$ distinct samples from a single biological replicate. *$p < 0.05$ and **$p < 0.005$ compared to cells are treated without an inhibitor. (B) Western blot demonstrating extraction of the whole-cell lysate and cytosolic fraction with RIPA and digitonin buffer, respectively. Erk 1/2 is a cytosolic marker, whereas Rab5 is a late-endosomal marker. Lysates shown are from untreated cells, as well as cells treated with PMO-D-Bpep and PMO-D-R8. (C, D) Example MALDI spectra following uptake analysis of lysates from (B) containing PMO-D-Bpep and PMO-D-R8, respectively. The intact construct was detected in the whole cell (top) as well as cytosolic (bottom) fractions.

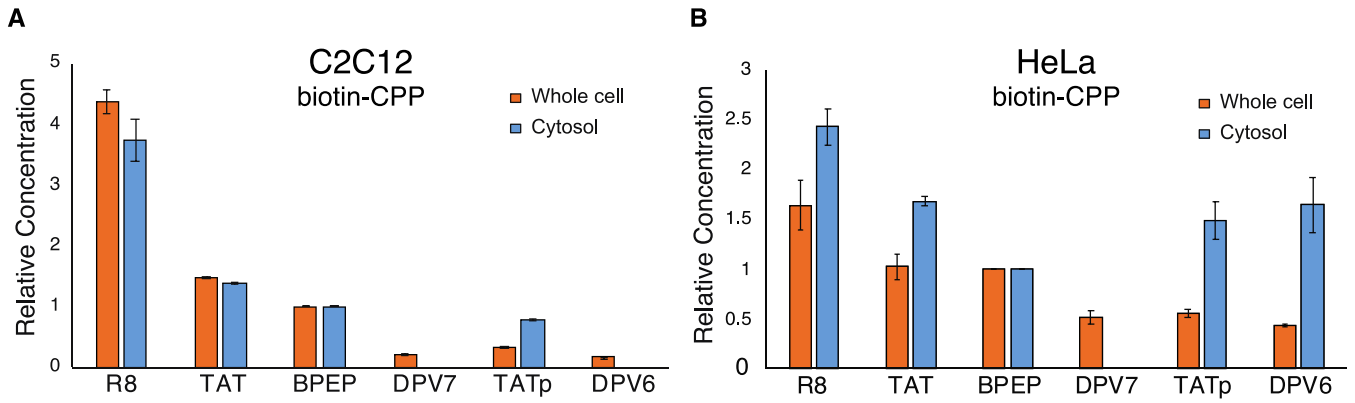

Figure 6. Uptake of biotin-CPPs can be profiled in different cell lines. (A) Bar graph showing concentrations of biotin-CPPs relative to BPEP in the whole cell and cytosolic extracts of C1C12 mouse myoblast cells following 1 h treatment at 37 °C. (B) Bar graph showing concentrations of biotin-CPPs in the whole cell and cytosolic extracts of HeLa cells following 1 h treatment at 37 °C. Bars represent group mean ± SD $N = 2$ replicate samples. Relative concentration is normalized to Bpep.

chlorpromazine reduced activity in a dose-dependent manner (Figure 5A) without demonstrating membrane toxicity (SI). Chlorpromazine is an inhibitor of clathrin-mediated endocytosis and has previously been observed to inhibit the activity of similar PMO constructs. While it is possible that multiple uptake mechanisms are occurring, these PMO−CPP conjugates are likely taken up by active transport.

Knowing that PMO−CPPs enter via endocytosis, we assert that extracting the cytosol and comparing it to the whole-cell lysate is critical when evaluating the relative concentrations of constructs internalized into cells. Not all endocytosed compounds are able to escape the endosome, and endosomal entrapment would lead to less active PMO delivered into the cytosol, measured by a lower cytosolic concentration relative to the whole-cell lysate. Therefore, we then extracted biotinylated PMO−CPPs from the cytosol as well as the whole-cell lysate following internalization and detected them by Western blot and MALDI. Individually, we incubated PMO-D-R8 or PMO-D-Bpep at 5 μM with HeLa cells in a 12-well plate for 1 h before washing with heparin and digesting with trypsin. The cytosol was extracted using Digitonin buffer, which selectively permeabilizes the outer membrane. RIPA buffer was used to prepare whole-cell lysates. To confirm cytosolic extraction, a portion of each sample was analyzed via Western blot using a cytosolic marker (Erk 1/2) and a late-endosomal marker (Rab5). The samples of the cytosolic extract from both treated and untreated cells have markedly reduced Rab5, while all samples contain Erk 1/2 (Figure 5B). Trace contamination of Rab5 is observed in the cytosolic extract, although the amount is significantly reduced compared to the whole-cell lysate. Finally, as with biotinylated peptides, PMO−CPPs were then extracted from the samples with streptavidin-coated magnetic Dynabeads, washed extensively, and analyzed via MALDI-TOF. We indeed detected PMO-D-R8 and PMO-D-Bpep in their respective samples, presenting the first instance of an intact peptide−oligonucleotide conjugate being extracted from cells and analyzed by mass spectrometry (Figure 5C,D). Moreover, we found that incubation at a lower temperature appeared to inhibit cytosolic localization of PMO-D-CPPs but resulted in equal relative concentrations between the whole cell and cytosolic fractions for biotin-D-CPPs, which may be able to passively diffuse through the membrane (SI).

Next, we expanded the analytes tested and profiled the uptake of six biotin-D-CPPs in the cytosol of distinct cell lines.

https://doi.org/10.1021/acsbiomedchemau.1c00053
ACS Bio Med Chem Au 2022, 2, 150−160

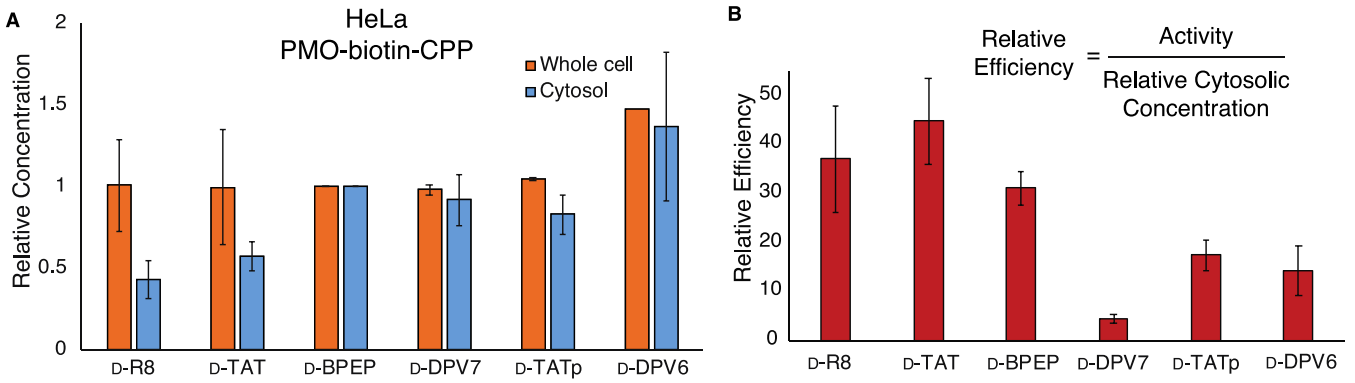

Figure 7. Mass spectrometry-based profiling combined with an activity gives a new efficiency metric for PMO−CPPs. (A) Bar graph showing the concentrations of PMO−biotin−CPPs relative to BPEP in the whole cell and cytosolic extracts of Hela cells. Relative concentration is normalized to BPEP. (B) Bar graph showing relative efficiency (PMO activity/relative cytosolic concentration) of PMO−CPPs. Bars show group mean ± SD, $N = 2$ distinct samples from a single biological replicate, except for the whole-cell condition of (A) in which $N = 2$ distinct samples from two independent biological replicates.

Biotin-D-R8, TAT, Bpep, DPV7, TATp, and DPV6 were profiled by MALDI in both HeLa (Figure 6A) and C2C12 mouse myoblast (Figure 6B) cell lines. We observed different uptake patterns between the two cell lines; polyarginine was significantly more abundant in C2C12 cells compared to the other peptides, and DPV6 and DPV7 were not detected in the cytosol. In HeLa, polyarginine had the highest relative concentration in both cytosol and whole cell, and DPV7 was again not detected in the cytosol. However, TAT, TATp, and DPV6 all had similar relative cytosolic concentrations. With these experiments, we demonstrated that this profiling platform could determine the relative concentration of six intact peptides extracted from whole cell and cytosol of two distinct cell lines.

Finally, we profiled the uptake of six PMO-D-CPPs. PMO-D-R8, TAT, BPEP, DPV7, TATp, and DPV6 were profiled in HeLa cells as usual. The extraction of cytosol was confirmed by Western blot (SI), and the samples were analyzed by MALDI. Relative concentrations were normalized to BPEP. In the whole-cell extract, the relative concentrations were generally consistent across peptides, with DPV6 having 1.5-fold higher relative concentration. On the other hand, relative concentrations in the cytosol were lower for the polyarginine peptides R8 and TAT and highest for BPEP and DPV6 (Figure 7A). By comparing the relative cytosolic concentration to overall peptide activity, relative efficiencies introduce a suitable metric for determining which of the six CPPs can effectively deliver PMO for nuclear splice-correction activity (Figure 7B).

CONCLUSIONS

Here, we show that the all-D version of several known cell-penetrating peptides can deliver an antisense oligonucleotide to the nucleus of cells with similar efficiency to their native L-form. While the respective activities were nearly identical in cells, D-forms were resistant to serum proteolysis. This stability enabled the recovery and mass spectrometric analysis of D-peptides from cytosolic and whole-cell lysates. By comparing PMO activity to relative internalized concentrations, we obtained a metric for PMO delivery efficiency.

While it would not be expected that the mirror-image versions of all CPPs would retain delivery activity, striking similarities observed for the mirror-image peptides selected in this study suggest that D-peptides should be studied further. Despite the similar activity in cells, the difference in proteolytic stability indicates the potential for differential activities in animals. Proteolytic degradation of peptide therapeutics has been considered a major weakness limiting therapeutic investigation.[44] However, mutations to D-amino acids, or the study of entirely D-peptides, has the potential to improve the pharmacokinetic properties of proteinogenic therapies. Avoidance of cleavage sites can enhance proteolytic stability and half-life in vivo and can be achieved by integration of unnatural amino acids, including D-amino acids.[45] An all-D polyproline CPP was shown to be efficacious in mice,[18] and PMO-D-CPPs were previously found to be the most stable among tested B-peptide analogues.[15] Moreover, it is likely that intact PMO−CPP conjugates are able to enter the nucleus as opposed to a cleaved PMO only.[22] Despite these promising findings, the activities of PMO-D-CPPs had not been previously explored. We found that, in HeLa cells, several CPP sequences had nearly identical delivery activities in their D- and L-forms, while the D-form remained proteolytically stable.

Besides potential in vivo applications, the proteostability of D-peptides also simplified their direct analysis by mass spectrometry following recovery from biological milieu. Previous reports demonstrated that biotinylated L-peptides could be recovered from inside the whole-cell lysate and quantified by MALDI-ToF, and cleavage products were identified and accounted for.[7,34] Here, by focusing only on fully intact constructs, we analyzed a mixture of six individual biotinylated D-peptides from inside cells by observing only the intact parent ions. Moreover, we demonstrated relative quantification of a mixture of biotinylated peptides recovered from the cytosolic extract. Analysis of the cytosolic portion is critical when studying and developing cell-penetrating peptides, considering that the whole-cell uptake does not correlate with cytosolic delivery due to the possibility of endosomal entrapment.

Finally, we showed relative quantification of intact biotinylated PMO-D-CPPs in the whole-cell lysate. By combining relative internal concentrations with PMO delivery activity, we obtained a metric for relative delivery efficiency. Delivery efficiency would be a useful metric for comparing CPPs delivering active therapeutic cargo as it takes into account both the activity of the cargo as well as the internal concentration. A highly efficient peptide would have high activity with low internal concentration and thus a high relative

https://doi.org/10.1021/acsbiomedchemau.1c00053
ACS Bio Med Chem Au 2022, 2, 150−160

efficiency. This metric decouples activity measurements from endosomal escape, allowing the direct comparison of cytosolic concentration and activity. Using these metrics when investigating CPPs would be useful in narrowing the scope of sequences early in development to exclude sequences that accumulate in the endosomes or otherwise do not efficiently deliver active cargo.

Exploration of the mirror-image CPPs would enter into a largely untapped chemical space. We recently described a machine learning-based platform for the discovery of nuclear-targeting peptides containing unnatural amino acids.[23] While the unnatural residues included in this work were non-α-amino acids, future applications of this method could include D-amino acid substitutions or fully mirror-image CPPs to discover highly active, novel sequences that are completely stable.

EXPERIMENTAL SECTION

Fast-Flow Peptide Synthesis

Peptides were synthesized on a 0.1 mmol scale using an automated[46] fast-flow peptide synthesizer for L-peptides and a semiautomated[47] fast-flow peptide synthesizer for D-peptides. Automated synthesis conditions were used as previously reported. Briefly, a 100 mg portion of ChemMatrix Rink Amide HYR resin was loaded into a reactor maintained at 90 °C. All reagents were flowed at 40 mL/min with HPLC pumps through a stainless-steel loop maintained at 90 °C before introduction into the reactor. For each coupling, 10 mL of a solution containing 0.4 M amino acid and 0.38 M HATU in DMF was mixed with 600 μL of diisopropylethylamine and delivered to the reactor. Fmoc removal was accomplished using 10.4 mL of 20% (v/v) piperidine. Between each step, DMF (15 mL) was used to wash out the reactor. To couple unnatural amino acids or to cap the peptide (e.g., with 4-pentynoic acid), the resin was incubated for 30 min at room temperature with amino acid (1 mmol) dissolved in 2.5 mL of 0.4 M HATU in DMF with 500 μL of diisopropylethylamine. After completion of the synthesis, the resin was washed three times with dichloromethane and dried under vacuum.

The semiautomated synthesis was carried out as previously described.[47] One millimole of amino acid was combined with 2.5 mL of 0.4 M HATU and 500 μL of DIEA and mixed before being delivered to the reactor containing resin via a syringe pump at 6 mL/min. The reactor was submerged in a water bath heated to 70 °C. An HPLC pump delivered either DMF (20 mL) for washing or 20% piperidine/DMF (6.7 mL) for Fmoc deprotection, at 20 mL/min.

Peptide Cleavage and Deprotection. Each peptide was subjected to simultaneous global side-chain deprotection and cleavage from the resin by treatment with 5 mL of 94% trifluoroacetic acid (TFA), 2.5% thioanisole, 2.5% water, and 1% triisopropylsilane (TIPS) (v/v) at room temperature for 2−4 h. The cleavage cocktail was first concentrated by bubbling N_2 through the mixture, and the cleaved peptide was precipitated and triturated with 40 mL of cold ether (chilled in dry ice). The crude product was pelleted by centrifugation for 3 min at 4 000 rpm, and the ether was decanted. This wash step was repeated two more times. After the third wash, the pellet was dissolved in 50% water and 50% acetonitrile containing 0.1% TFA, filtered through a fritted syringe to remove the resin and lyophilized.

Peptide Purification. The peptides were dissolved in water and acetonitrile containing 0.1% TFA, filtered through a 0.22 μm nylon filter, and purified by mass-directed semipreparative reversed-phase HPLC. Solvent A was water with 0.1% TFA additive, and Solvent B was acetonitrile with 0.1% TFA additive. A linear gradient that changed at a rate of 0.5% B/min was used. Most of the peptides were purified on an Agilent Zorbax SB C18 column: 9.4 mm × 250 mm, 5 μm. Using mass data about each fraction from the instrument, only pure fractions were pooled and lyophilized. The purity of the fraction pool was confirmed to be >95% by LC-MS.

PMO-DBCO Synthesis. PMO IVS2-654 (50 mg, 8 μmol) was dissolved in 150 μL of DMSO. To the solution was added a solution containing 2 equivalents of dibenzocyclooctyne acid (5.3 mg, 16 μmol) activated with HBTU (37.5 μL of 0.4 M HBTU in DMF, 15 μmol) and DIEA (2.8 μL, 16 μmol) in 40 μL of DMF (final reaction volume = 0.23 mL). The reaction proceeded for 25 min before being quenched with 1 mL of water and 2 mL of ammonium hydroxide. The ammonium hydroxide hydrolyzed any ester formed during the course of the reaction. After 1 h, the solution was diluted to 40 mL in water/acetonitrile and purified using reverse-phase HPLC (Agilent Zorbax SB C3 column: 21.2 mm × 100 mm, 5 μm) and a linear gradient from 2 to 60% B (solvent A: water; solvent B: acetonitrile) over 58 min (1% B/min). Using mass data about each fraction from the instrument, only pure fractions were pooled and lyophilized. The purity of the fraction pool was confirmed to be >95% by LC-MS.

Conjugation to Peptides. PMO-DBCO (1 equiv, 5 mM, water) was conjugated to azido-peptides (1.5 equiv, 5 mM, water) at room temperature for 2 h. Reaction progress was monitored by LC-MS and purified when PMO-DBCO was consumed. Purification was conducted using mass-directed HPLC (Solvent A: 100 mM ammonium acetate in water, Solvent B: acetonitrile) with a linear gradient that changed at a rate of 0.5% B/min, on an Agilent Zorbax SB C13 column: 9.4 mm × 250 mm, 5 μm. Using mass data about each fraction from the instrument, only pure fractions were pooled and lyophilized. The purity of the fraction pool was confirmed to be >95% by both LC-MS and UV.

EGFP Assay

HeLa 654 cells were maintained in minimum essential media (MEM) supplemented with 10% (v/v) fetal bovine serum (FBS) and 1% (v/v) penicillin−streptomycin at 37 °C and 5% CO_2. Eighteen hours prior to treatment, the cells were plated at a density of 5 000 cells per well in a 96-well plate in MEM supplemented with 10% FBS and 1% penicillin−streptomycin.

PMO−peptides were dissolved in cation-free PBS at a concentration of 1 mM (determined by UV) before being diluted in MEM. Cells were incubated at the designated concentrations for 22 h at 37 °C and 5% CO_2. The treatment media was removed, and the cells were washed once before being incubated with 0.25% trypsin-EDTA for 15 min at 37 °C and 5% CO_2. Lifted cells were transferred to a *V*-bottom 96-well plate and washed once with PBS, before being resuspended in PBS containing 2% FBS and 2 μg/mL propidium iodide (PI). Flow cytometry analysis was carried out on a BD LSRII flow cytometer at the Koch Institute. Gates were applied to the data to ensure that cells that were positive for propidium iodide or had forward/side scatter readings that were sufficiently different from the main cell population were excluded. Each sample was capped at 5 000 gated events.

Analysis was conducted using Graphpad Prism 7 and FlowJo. For each sample, the mean fluorescence intensity (MFI) and the number of gated cells were measured. To report activity, triplicate MFI values were averaged and normalized to the PMO alone condition.

Uptake Assay

The uptake assay was adapted from a previously reported protocol and is detailed fully in the Supporting Information.[35] Briefly, cells were plated in a 12-well plate the evening before the experiment. On the day of the experiment, cells were treated at varying concentrations of PMO−biotin−peptide or biotin−peptide at varying temperatures and durations. Treatment media was removed, and cells were washed with fresh media before incubating with porcine heparin for 5 min to dissociate membrane-bound peptide. Cells were lifted and membrane-bound peptide was cleaved by incubation in trypsin for 5 min. Collected cells were pelleted and washed before being digested with RIPA buffer (for the whole-cell extract) or digitonin buffer (for cytosolic extract) on ice. The supernatant was collected, and the protein concentration was quantified using a BCA protein assay kit. A portion of some samples was retained for analysis by Western blot. The remaining supernatant was incubated with magnetic streptavidin Dynabeads overnight at 4 °C.

https://doi.org/10.1021/acsbiomedchemau.1c00053
ACS Bio Med Chem Au 2022, 2, 150−160

Dynabeads were washed with a series of buffers: 2 × 100 μL Buffer A (50 mM Tris-HCl (pH 7.4) and 0.1 mg/mL BSA), 2 × 100 μL Buffer B (50 mM Tris-HCl (pH 7.4), 0.1 mg/mL BSA, and 0.1% SDS), 2 × 100 μL Buffer C (50 mM Tris-HCl (pH 7.4), 0.1 mg/mL BSA, and 1 M NaCl), and 2 × 100 μL water. The washed beads were then resuspended in the CHCA MALDI matrix and plated directly on a MALDI plate. The plate was analyzed using MALDI-ToF on a high-resolution Bruker Autoflex LRF speed mass spectrometer in a linear positive mode.

Relative concentrations of peptides in the mixture were determined as follows. Analytes in a mixture ionizing according to their response factor (F). F was determined by normalizing the intensities of each analyte to one analyte in the control sample, where the concentration of each analyte is arbitrarily set to 1. The values of F were then used in the experimental spectra containing the same mixture of analytes to determine their relative concentrations.

$$\frac{I_x}{[X]} = F\left(\frac{I_s}{[S]}\right)$$

Statistics

Statistical analysis and graphing were performed using Prism (Graphpad) or Excel (Microsoft). Concentration−response curves were fitted using Prism using nonlinear regression. The listed replicates for each experiment indicate the number of distinct samples measured for a given assay. Significance for activities between constructs was determined using a Student's two-sided, unpaired t-test.

■ ASSOCIATED CONTENT

Supporting Information

The Supporting Information is available free of charge at https://pubs.acs.org/doi/10.1021/acsbiomedchemau.1c00053.

Materials, LC-MS analysis (Section 1); activity and toxicity assays, serum stability assay (Section 2); methods for uptake assay, additional MALDI-ToF experiments (Section 3); gel images (Appendix I); and LC-MS characterization (Appendix II) (PDF)

■ AUTHOR INFORMATION

Corresponding Author

Bradley L. Pentelute − *Department of Chemistry, Massachusetts Institute of Technology, Cambridge, Massachusetts 02139, United States; The Koch Institute for Integrative Cancer Research, Massachusetts Institute of Technology, Cambridge, Massachusetts 02142, United States; Center for Environmental Health Sciences, Massachusetts Institute of Technology, Cambridge, Massachusetts 02139, United States; Broad Institute of MIT and Harvard, Cambridge, Massachusetts 02142, United States;* orcid.org/0000-0002-7242-801X; Email: blp@mit.edu

Authors

Carly K. Schissel − *Department of Chemistry, Massachusetts Institute of Technology, Cambridge, Massachusetts 02139, United States;* orcid.org/0000-0003-0773-5168

Charlotte E. Farquhar − *Department of Chemistry, Massachusetts Institute of Technology, Cambridge, Massachusetts 02139, United States*

Annika B. Malmberg − *Sarepta Therapeutics, Cambridge, Massachusetts 02142, United States*

Andrei Loas − *Department of Chemistry, Massachusetts Institute of Technology, Cambridge, Massachusetts 02139, United States;* orcid.org/0000-0001-5640-1645

Complete contact information is available at: https://pubs.acs.org/10.1021/acsbiomedchemau.1c00053

Notes

The authors declare the following competing financial interest(s): B.L.P. is a co-founder of Amide Technologies and Resolute Bio, two companies that focus on the development of protein and peptide therapeutics. Sarepta Therapeutics has filed a provisional patent application related to the compounds described in this work.

All data is available in the main text or the Supporting Information

■ ACKNOWLEDGMENTS

This research was funded by Sarepta Therapeutics. C.K.S. (4000057398) and C.E.F. (4000057441) acknowledge the National Science Foundation Graduate Research Fellowship (NSF Grant no. 1122374) for research support. The authors thank the Swanson Biotechnology Center Flow Cytometry Facility at the Koch Institute for the use of their flow cytometers (NCI Cancer Center Support Grant P30-CA14051) and MIT's Department of Chemistry Instrumentation Facility for the use of the MALDI-ToF.

■ REFERENCES

(1) Wolfe, J. M.; Fadzen, C. M.; Holden, R. L.; Yao, M.; Hanson, G. J.; Pentelute, B. L. Perfluoroaryl Bicyclic Cell-Penetrating Peptides for Delivery of Antisense Oligonucleotides. *Angew. Chem., Int. Ed.* **2018**, *57*, 4756−4759.

(2) Oehlke, J.; Scheller, A.; Wiesner, B.; Krause, E.; Beyermann, M.; Klauschenz, E.; Melzig, M.; Bienert, M. Cellular Uptake of an α-Helical Amphipathic Model Peptide with the Potential to Deliver Polar Compounds into the Cell Interior Non-Endocytically. *Biochim. Biophys. Acta, Biomembr.* **1998**, *1414*, 127−139.

(3) Margus, H.; Padari, K.; Pooga, M. Cell-Penetrating Peptides as Versatile Vehicles for Oligonucleotide Delivery. *Mol. Ther.* **2012**, *20*, 525−533.

(4) Reissmann, S. Cell Penetration: Scope and Limitations by the Application of Cell-penetrating Peptides. *J. Pept. Sci.* **2014**, *20*, 760−784.

(5) Fischer, R.; Waizenegger, T.; Köhler, K.; Brock, R. A Quantitative Validation of Fluorophore-Labelled Cell-Permeable Peptide Conjugates: Fluorophore and Cargo Dependence of Import. *Biochim. Biophys. Acta, Biomembr.* **2002**, *1564*, 365−374.

(6) Lindgren, M. E.; Hällbrink, M. M.; Elmquist, A. M.; Langel, U. Passage of Cell-Penetrating Peptides across a Human Epithelial Cell Layer in Vitro. *Biochem. J.* **2004**, *377*, 69−76.

(7) Illien, F.; Rodriguez, N.; Amoura, M.; Joliot, A.; Pallerla, M.; Cribier, S.; Burlina, F.; Sagan, S. Quantitative Fluorescence Spectroscopy and Flow Cytometry Analyses of Cell-Penetrating Peptides Internalization Pathways: Optimization, Pitfalls, Comparison with Mass Spectrometry Quantification. *Sci. Rep.* **2016**, *6*, No. 36938.

(8) Wolfe, J. M.; Fadzen, C. M.; Choo, Z.-N.; Holden, R. L.; Yao, M.; Hanson, G. J.; Pentelute, B. L. Machine Learning To Predict Cell-Penetrating Peptides for Antisense Delivery. *ACS Cent. Sci.* **2018**, *4*, 512−520.

(9) Baker, D. E. Eteplirsen. *Hosp. Pharm.* **2017**, *52*, 302−305.

(10) Lim, K. R. Q.; Maruyama, R.; Yokota, T. Eteplirsen in the Treatment of Duchenne Muscular Dystrophy. *Drug Des., Dev. Ther.* **2017**, *11*, 533−545.

(11) SareptaTherapeutics Announces Positive Clinical Results from MOMENTUM, a Phase 2Clinical Trial of SRP-5051 in Patients with

Duchenne Muscular DystrophyAmenable to Skipping Exon 51. http://www.globenewswire.com/news-release/2020/12/07/2140613/0/en/Sarepta-Therapeutics-Announces-Positive-Clinical-Results-from-MOMENTUM-a-Phase-2-Clinical-Trial-of-SRP-5051-in-Patients-with-Duchenne-Muscular-Dystrophy-Amenable-to-Skipping-Exon-5.html (accessed December 07, 2020).
(12) Kurrikoff, K.; Vunk, B.; Langel, Ü. Status Update in the Use of Cell-Penetrating Peptides for the Delivery of Macromolecular Therapeutics. *Expert Opin. Biol. Ther.* **2021**, *21*, 361−370.
(13) Dintzis, H. M.; Symer, D. E.; Dintzis, R. Z.; Zawadzke, L. E.; Berg, J. M. A Comparison of the Immunogenicity of a Pair of Enantiomeric Proteins. *Proteins: Struct., Funct., Genet.* **1993**, *16*, 306−308.
(14) Kroenke, M. A.; Weeraratne, D. K.; Deng, H.; Sloey, B.; Subramanian, R.; Wu, B.; Serenko, M.; Hock, M. B. Clinical Immunogenicity of the D-Amino Acid Peptide Therapeutic Etelcalcetide: Method Development Challenges and Anti-Drug Antibody Clinical Impact Assessments. *J. Immunol. Methods* **2017**, *445*, 37−44.
(15) Najjar, K.; Erazo-Oliveras, A.; Brock, D. J.; Wang, T.-Y.; Pellois, J.-P. An L- to d-Amino Acid Conversion in an Endosomolytic Analog of the Cell-Penetrating Peptide TAT Influences Proteolytic Stability, Endocytic Uptake, and Endosomal Escape. *J. Biol. Chem.* **2017**, *292*, 847−861.
(16) Ma, Y.; Gong, C.; Ma, Y.; Fan, F.; Luo, M.; Yang, F.; Zhang, Y.-H. Direct Cytosolic Delivery of Cargoes in Vivo by a Chimera Consisting of D- and L-Arginine Residues. *J. Controlled Release* **2012**, *162*, 286−294.
(17) Henriques, S. T.; Peacock, H.; Benfield, A. H.; Wang, C. K.; Craik, D. J. Is the Mirror Image a True Reflection? Intrinsic Membrane Chirality Modulates Peptide Binding. *J. Am. Chem. Soc.* **2019**, *141*, 20460−20469.
(18) Pujals, S.; Sabidó, E.; Tarragó, T.; Giralt, E. All-D Proline-Rich Cell-Penetrating Peptides: A Preliminary in Vivo Internalization Study. *Biochem. Soc. Trans.* **2007**, *35*, 794−796.
(19) Ito, S.; Torii, Y.; Chikamatsu, S.; Harada, T.; Yamaguchi, S.; Ogata, S.; Sonoda, K.; Wakayama, T.; Masuda, T.; Ohtsuki, S. Oral Coadministration of Zn-Insulin with d-Form Small Intestine-Permeable Cyclic Peptide Enhances Its Blood Glucose-Lowering Effect in Mice. *Mol. Pharmaceutics* **2021**, *18*, 1593−1603.
(20) Verdurmen, W. P. R.; Bovee-Geurts, P. H.; Wadhwani, P.; Ulrich, A. S.; Hällbrink, M.; van Kuppevelt, T. H.; Brock, R. Preferential Uptake of L- versus D-Amino Acid Cell-Penetrating Peptides in a Cell Type-Dependent Manner. *Chem. Biol.* **2011**, *18*, 1000−1010.
(21) Knox, S. L.; Wissner, R.; Piszkiewicz, S.; Schepartz, A. Cytosolic Delivery of Argininosuccinate Synthetase Using a Cell-Permeant Miniature Protein. *ACS Cent. Sci.* **2021**, *7*, 641−649.
(22) Fadzen, C. M.; Holden, R. L.; Wolfe, J. M.; Choo, Z.-N.; Schissel, C. K.; Yao, M.; Hanson, G. J.; Pentelute, B. L. Chimeras of Cell-Penetrating Peptides Demonstrate Synergistic Improvement in Antisense Efficacy. *Biochemistry* **2019**, *58*, 3980−3989.
(23) Schissel, C. K.; Mohapatra, S.; Wolfe, J. M.; Fadzen, C. M.; Bellovoda, K.; Wu, C.-L.; Wood, J. A.; Malmberg, A. B.; Loas, A.; Gómez-Bombarelli, R.; Pentelute, B. L. Deep Learning to Design Nuclear-Targeting Abiotic Miniproteins. *Nat. Chem.* **2021**, *13*, 992−1000.
(24) Youngblood, D. S.; Hatlevig, S. A.; Hassinger, J. N.; Iversen, P. L.; Moulton, H. M. Stability of Cell-Penetrating Peptide−Morpholino Oligomer Conjugates in Human Serum and in Cells. *Bioconjugate Chem.* **2007**, *18*, 50−60.
(25) Sazani, P.; Gemignani, F.; Kang, S.-H.; Maier, M. A.; Manoharan, M.; Persmark, M.; Bortner, D.; Kole, R. Systemically Delivered Antisense Oligomers Upregulate Gene Expression in Mouse Tissues. *Nat. Biotechnol.* **2002**, *20*, 1228−1233.
(26) Erazo-Oliveras, A.; Muthukrishnan, N.; Baker, R.; Wang, T.-Y.; Pellois, J.-P. Improving the Endosomal Escape of Cell-Penetrating Peptides and Their Cargos: Strategies and Challenges. *Pharmaceuticals* **2012**, *5*, 1177−1209.
(27) Holden, P.; Horton, W. A. Crude Subcellular Fractionation of Cultured Mammalian Cell Lines. *BMC Res. Notes* **2009**, *2*, No. 243.
(28) Peraro, L.; Deprey, K. L.; Moser, M. K.; Zou, Z.; Ball, H. L.; Levine, B.; Kritzer, J. A. Cell Penetration Profiling Using the Chloroalkane Penetration Assay. *J. Am. Chem. Soc.* **2018**, *140*, 11360−11369.
(29) Schmidt, S.; Adjobo-Hermans, M. J. W.; Wallbrecher, R.; Verdurmen, W. P. R.; Bovée-Geurts, P. H. M.; van Oostrum, J.; Milletti, F.; Enderle, T.; Brock, R. Detecting Cytosolic Peptide Delivery with the GFP Complementation Assay in the Low Micromolar Range. *Angew. Chem., Int. Ed.* **2015**, *54*, 15105−15108.
(30) Peier, A.; Ge, L.; Boyer, N.; Frost, J.; Duggal, R.; Biswas, K.; Edmondson, S.; Hermes, J. D.; Yan, L.; Zimprich, C.; Sadruddin, A.; Kristal Kaan, H. Y.; Chandramohan, A.; Brown, C. J.; Thean, D.; Lee, X. E.; Yuen, T. Y.; Ferrer-Gago, F. J.; Johannes, C. W.; Lane, D. P.; Sherborne, B.; Corona, C.; Robers, M. B.; Sawyer, T. K.; Partridge, A. W. NanoClick: A High Throughput, Target-Agnostic Peptide Cell Permeability Assay. *ACS Chem. Biol.* **2021**, *16*, 293−309.
(31) Teo, S. L. Y.; Rennick, J. J.; Yuen, D.; Al-Wassiti, H.; Johnston, A. P. R.; Pouton, C. W. Unravelling Cytosolic Delivery of Cell Penetrating Peptides with a Quantitative Endosomal Escape Assay. *Nat. Commun.* **2021**, *12*, No. 3721.
(32) Wissner, R. F.; Steinauer, A.; Knox, S. L.; Thompson, A. D.; Schepartz, A. Fluorescence Correlation Spectroscopy Reveals Efficient Cytosolic Delivery of Protein Cargo by Cell-Permeant Miniature Proteins. *ACS Cent. Sci.* **2018**, *4*, 1379−1393.
(33) Bucknall, M.; Fung, K. Y.; Duncan, M. W. Practical Quantitative Biomedical Applications of MALDI-TOF Mass Spectrometry. *J. Am. Soc. Mass Spectrom.* **2002**, *13*, 1015−1027.
(34) Burlina, F.; Sagan, S.; Bolbach, G.; Chassaing, G. Quantification of the Cellular Uptake of Cell-Penetrating Peptides by MALDI-TOF Mass Spectrometry. *Angew. Chem., Int. Ed.* **2005**, *44*, 4244−4247.
(35) Burlina, F.; Sagan, S.; Bolbach, G.; Chassaing, G. A Direct Approach to Quantification of the Cellular Uptake of Cell-Penetrating Peptides Using MALDI-TOF Mass Spectrometry. *Nat. Protoc.* **2006**, *1*, 200−205.
(36) Aubry, S.; Aussedat, B.; Delaroche, D.; Jiao, C.-Y.; Bolbach, G.; Lavielle, S.; Chassaing, G.; Sagan, S.; Burlina, F. MALDI-TOF Mass Spectrometry: A Powerful Tool to Study the Internalization of Cell-Penetrating Peptides. *Biochim. Biophys. Acta, Biomembr.* **2010**, *1798*, 2182−2189.
(37) Ho, H.-P.; Rathod, P.; Louis, M.; Tada, C. K.; Rahaman, S.; Mark, K. J.; Leng, J.; Dana, D.; Kumar, S.; Lichterfeld, M.; Chang, E. J. Studies on Quantitative Phosphopeptide Analysis by MALDI Mass Spectrometry Without Label, Chromatography or Calibration Curves. *Rapid Commun. Mass Spectrom.* **2014**, *28*, 2681−2689.
(38) Aussedat, B.; Sagan, S.; Chassaing, G.; Bolbach, G.; Burlina, F. Quantification of the Efficiency of Cargo Delivery by Peptidic and Pseudo-Peptidic Trojan Carriers Using MALDI-TOF Mass Spectrometry. *Biochim. Biophys. Acta, Biomembr.* **2006**, *1758*, 375−383.
(39) Bode, S. A.; Thévenin, M.; Bechara, C.; Sagan, S.; Bregant, S.; Lavielle, S.; Chassaing, G.; Burlina, F. Self-Assembling Mini Cell-Penetrating Peptides Enter by Both Direct Translocation and Glycosaminoglycan-Dependent Endocytosis. *Chem. Commun.* **2012**, *48*, 7179−7181.
(40) Aussedat, B.; Dupont, E.; Sagan, S.; Joliot, A.; Lavielle, S.; Chassaing, G.; Burlina, F. Modifications in the Chemical Structure of Trojan Carriers: Impact on Cargo Delivery. *Chem. Commun.* **2008**, 1398−1400.
(41) Brock, R. The Uptake of Arginine-Rich Cell-Penetrating Peptides: Putting the Puzzle Together. *Bioconjugate Chem.* **2014**, *25*, 863−868.
(42) Fuchs, S. M.; Raines, R. T. Polyarginine as a Multifunctional Fusion Tag. *Protein Sci.* **2005**, *14*, 1538−1544.
(43) Richard, J. P.; Melikov, K.; Vives, E.; Ramos, C.; Verbeure, B.; Gait, M. J.; Chernomordik, L. V.; Lebleu, B. Cell-Penetrating Peptides. A Reevaluation of the Mechanism of Cellular Uptake. *J. Biol. Chem.* **2003**, *278*, 585−590.

https://doi.org/10.1021/acsbiomedchemau.1c00053
ACS Bio Med Chem Au 2022, 2, 150−160

(44) Böttger, R.; Hoffmann, R.; Knappe, D. Differential Stability of Therapeutic Peptides with Different Proteolytic Cleavage Sites in Blood, Plasma and Serum. *PLoS One* **2017**, *12*, No. e0178943.
(45) Werner, H. M.; Cabalteja, C. C.; Horne, W. S. Peptide Backbone Composition and Protease Susceptibility: Impact of Modification Type, Position, and Tandem Substitution. *ChemBioChem* **2016**, *17*, 712−718.
(46) Hartrampf, N.; Saebi, A.; Poskus, M.; Gates, Z. P.; Callahan, A. J.; Cowfer, A. E.; Hanna, S.; Antilla, S.; Schissel, C. K.; Quartararo, A. J.; Ye, X.; Mijalis, A. J.; Simon, M. D.; Loas, A.; Liu, S.; Jessen, C.; Nielsen, T. E.; Pentelute, B. L. Synthesis of Proteins by Automated Flow Chemistry. *Science* **2020**, *368*, 980−987.
(47) Simon, M. D.; Heider, P. L.; Adamo, A.; Vinogradov, A. A.; Mong, S. K.; Li, X.; Berger, T.; Policarpo, R. L.; Zhang, C.; Zou, Y.; Liao, X.; Spokoyny, A. M.; Jensen, K. F.; Pentelute, B. L. Rapid Flow-Based Peptide Synthesis. *ChemBioChem* **2014**, *15*, 713−720.

https://doi.org/10.1021/acsbiomedchemau.1c00053
ACS Bio Med Chem Au 2022, 2, 150−160